Journal of Materials Chemistry A

Accepted Manuscript

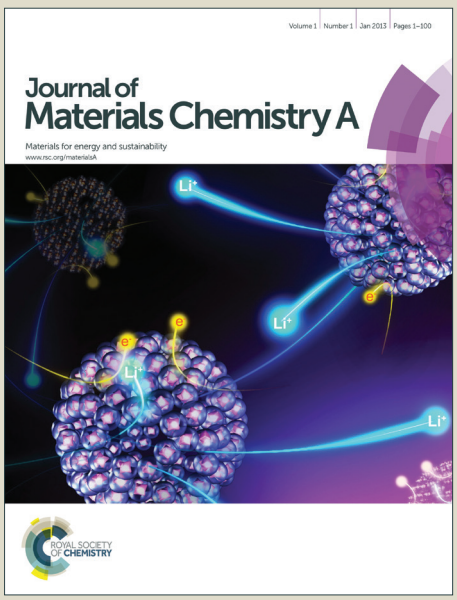

ROYAL SOCIETY OF CHEMISTRY

www.rsc.org/materialsA

The effect of high external pressure on structure and stability of MOF α-$Mg_3(HCOO)_6$ probed by *in situ* Raman and FT-IR Spectroscopy

Haiyan Mao[a,b], Jun Xu[b], Yue Hu[b], Yining Huang[b,*] and Yang Song[b,*]

[a]College of Materials Science and Engineering, Nanjing Forestry University, 159 Longpan Road, 210037, Nanjing, China

[b]Department of Chemistry, The University of Western Ontario, London ON N6A 5B7 Canada

*Corresponding authors. E-mail: yhuang@uwo.ca; yang.song@uwo.ca

Abstract

α-magnesium formate [α-$Mg_3(HCOO)_6$], a representative lightweight Mg-based metal-organic framework (MOF) has the desirable properties of permanent porosity, unique stability and adsorption capacities for small molecules. Using *in situ* infrared (IR) and Raman spectroscopy, we investigated the structure and stability of the α-$Mg_3(HCOO)_6$ framework at high pressures up to 13 GPa. We found that the framework structure was chemically stable under compression, while an irreversible crystal-to-crystal structural transition was observed above 2 GPa. This new phase is likely isostructural with microporous β-$Mg_3(HCOO)_6$. In contrast, the α-$Mg_3(HCOO)_6$ framework loaded with guest molecules such as DMF and benzene exhibit higher stability to external pressure. Neither a new crystalline phase nor an amorphous material was observed under pressure up to 13 GPa.

1. Introduction

MOFs (Metal-organic frameworks) are a type of new hybrid porous materials, consisting of metal ions and organic linkers.[1] MOFs possess potential applications in various sectors such as separation, gas storage, catalysis and controlled drug delivery.[2, 3] Recently, the coordination chemistry of MOFs based on main-group metals, especially, light main group metals like Mg have drawn much attention, as they are inexpensive, nontoxic, and have low atomic weight.[4] Mallick et al.,[5] Rood et al.,[6] and Britt et al.[7] reported Mg-based MOFs such as Mg-MOF-74, α and γ- magnesium formate, all of which show good carbon dioxide and hydrogen adsorption capabilities. Microporous α-$Mg_3(HCOO)_6$ (or α-magnesium formate) is one of the typical Mg-based MOF and commercially available with the trade name Basosive M050.[8] This MOF is easy to synthesize on a large scale under solvent-free conditions using low-cost and nontoxic starting materials, (i.e., MgO and formic acid). Moreover, it shows permanent porosity, good stability in various solvents and the framework is also stable even after activation up to 400 °C.[6]

α-$Mg_3(HCOO)_6$ crystallizes in monoclinic space group $P2_1/n$.[6] This MOF has one dimensional channel (pore size: 4.5 × 5.5 Å) covered with oxygen atoms and C-H bonds on the surface of the channel (shown in Fig. 1a.). The framework contains interconnecting one-dimensional chains of edge-shared octahedra of Mg1 and Mg3 with vertex-shared MgO_6 octahedra of Mg2 and Mg4 via Mg1, forming narrow one-dimensional zig-zag channels along the *b* axis. All of the formate anions adopt similar binding modes, with one oxygen connecting to a single metal center (μ^1-O) and the second oxygen bridging between two other metals (μ^2-O) (Fig. 1b). There are three

different coordination environments for the metal centers. Mg1 bonds to six μ^2-O, Mg2 and Mg4 each bond to four μ^1-O and two μ^2-O, whereas Mg3 bonds to two μ^1-O and four μ^2-O (Fig. 1c).[6]

In addition to single crystal X-ray diffraction, several other experimental techniques such as solid-state nuclear magnetic resonance (SSNMR) and Infrared spectroscopy (IR) have been used to characterize this MOF. Xu et al.[4] performed ^{25}Mg SSNMR spectroscopy and resolved four different Mg sites. IR spectra was used by Rood et al.[6] to study α-$Mg_3(HCOO)_6$ loaded with dimethylformamide (DMF).

It is well known that external pressure can influence the structures of porous materials as well as their physical and chemical properties. Recently, several studies have been performed to study the structural flexibility of MOFs (e.g., MOF-5, Cu-btc, ZIF-8, (4-chloropyridinium)$_2$[CoX_4] (X=Cl, Br), etc.) under high pressure. [8-17] In particular, Espallargas et al. investigated the structures and intermolecular interactions of (4-chloropyridinium)$_2$[CoX_4] (X=Cl, Br) using single-crystal X-ray diffraction at the pressure up to 4.1 GPa.[17] Later high-pressure studies on MOF-5 suggest unusual compression behavior of the framework in terms of volume expansion due to the interaction with surrounding solvent in the relatively low pressure region (e.g., < 1.3 GPa) whereas compression to 3.2 GPa results in complete amorphization of the framework.[12] Hu et al. investigated the behavior of ZIF-8 structure and its application for CO_2 storage under high pressures by IR spectroscopy.[8, 14] Their work suggested that the empty ZIF-8 framework is stable under pressure up to 1.6 GPa. Cu-btc (copper(II)-benzene-1,3,5-tricarboxylate) framework was found to undergo a phase transition at a pressure of 3.9

GPa and exhibit a unique compressibility.[10,11] All these studies have demonstrated that it is important to study the MOF framework under high pressures as different MOFs exhibit different stability and flexibility under different pressures. Furthermore, it is well known that the pressure transmitting medium (PTM) can play a discriminating role in the pressure behavior of porous framework structures of MOFs.[17,18] In the present work, we examined the behavior of activated microporous α-$Mg_3(HCOO)_6$ and that loaded with guest molecules such as DMF and benzene under high external pressures using Infrared and Raman spectroscopy. These two guest molecules have different size and polarity and may have different effects on the framework. The particular attention was paid to the framework stability and possible phase transitions induced by pressures.

2. Experimental

The α-$Mg_3(HCOO)_6$ sample was synthesized according to the literature.[6] Powder X-ray diffraction (XRD) is used to confirm the phase purity of synthesized MOF. The sample activation was performed by drying the sample in an oven at 150 °C for 24 h. The benzene-loaded sample was prepared by soaking the sample in benzene.

A symmetric diamond anvil cell (DAC) equipped with two type-I diamonds each with 600 μm culet was used for the high-pressure Raman measurements, while a pair of type-II diamonds with a culet size of 400 μm was used for the IR measurements. The samples were loaded into the DAC without KBr and with KBr for Raman and IR measurement, respectively. A few ruby chips were used as a pressure calibration and carefully placed inside the gasket chamber. The pressure was determined according to the well-established ruby fluorescent method.[19]

Raman experiment was carried out with a customized Raman micro-spectroscopic

system. A 532 nm laser line from a diode-pumped solid-state laser with an output power of ~ 100 mW was used as the excitation source. The system was calibrated using neon lines with an uncertainty of ±1 cm^{-1}. As a result of the strong diamond T_{2g} Raman mode at 1334 cm^{-1}, the spectra were collected in ranges of 50 to 1200 cm^{-1} and 1370 to 3000 cm^{-1} in several dispersive collection windows. All Raman experiments were conducted at room temperature at pressures of up to ~ 4 GPa and duplicated for more than 3 times.

For IR experiments, a customized IR micro-spectroscopic system was used for all room-temperature IR absorption measurements. A commercial Fourier transform infrared (FT-IR) spectrometer (Model Vertex 80v) from Bruker Optics Inc. equipped with Globar mid-IR light source constituted the main component of the micro-IR system and was operated under a vacuum of < 5 mbar such that absorption by H_2O and CO_2 was efficiently removed.[20] The diameter of the IR beam was adjusted to be identical to the entire sample size (e.g., ~ 150 μm) by a series of iris apertures. The background spectrum, i.e., the absorption of diamond anvils loaded with KBr, but without any sample was divided from each sample spectrum to obtain the absorbance.

3. Results and discussion

3.1. Ambient-pressure Raman and IR spectra of activated and guest loaded frameworks

Activated α-$Mg_3(HCOO)_6$. The ambient pressure Raman and IR spectra of activated sample are depicted in Figs. 2 and 3. The spectral assignments are given in Table 1. In the Raman spectrum (Fig. 2), low-frequency bands in the region of 100-350 cm^{-1} are ascribed to Mg-O lattice mode vibrations according to the assignments for

magnesium acetates and other metal formats.[21, 22] The peaks at 779 and 792 cm^{-1} are assigned to the OCO symmetric bending modes, δ_s(OCO).[23] The peak at 1064 cm^{-1} is due to the C-H out of plane rocking (ρ_{op}(C-H)). The positions of the framework OCO symmetric stretching modes (ν_s(OCO)) were observed at 1375, 1398 and 1404 cm^{-1}.[23] The bands in the spectral region of 1630-1690 cm^{-1} originate from the OCO asymmetric stretching vibrations (ν_{as}(OCO)). Three sharp peaks at 2879, 2898 and 2931 cm^{-1} are ascribed to the C-H stretching ($\nu_{s,\ as}$(C-H)).[24] Observing well resolved multiple sharper peaks in the C-H stretching region suggests that the framework C-H fragments are highly isolated and non-interacting.

Supplementary to the Raman measurements, the ambient mid-IR spectrum is shown on the top of Fig. 3. Our ambient pressure IR spectrum is in good agreement with previously reported IR spectra of α-$Mg_3(HCOO)_6$ loaded with DMF and $Mg(HCOO)_2 \cdot H_2O$[6, 25] (shown in Table 1). The IR peaks at 1610 and 1685 cm^{-1} are attributed to ν_{as}(OCO). The ν_s(C-H) and ν_{as}(C-H) bands in both the IR and Raman spectra are located at high frequencies of around 2900 cm^{-1}. The peaks at 700 and 767 cm^{-1} are assigned to δ_s(OCO) according to the reference.[21] In addition, the peaks at 1368, 1379, 1385, 1396 and 1406 cm^{-1} are assigned to ν_s(OCO).[25]

Guests loaded α-$Mg_3(HCOO)_6$. The α-$Mg_3(HCOO)_6$ framework has a pore diameter of 6 Å , which provides enough space for guest molecules such as benzene and DMF to fit inside the channels. In the Raman spectrum of DMF loaded framework (Fig. 2 and Table 1), the peaks at 660 and 866 cm^{-1} are assigned to the O=C-N bending, δ(O=C-N), and C-N symmetric stretching ν_s(C-N) modes, respectively.[26] Compared to the Raman spectrum of activated framework, an additional peak at 1439 cm^{-1} can be assigned

to the δ(C-H) from DMF molecule.[27] Similarly, the bands at 1664, 1687 cm^{-1} are due to the ν_{as}(C=O) of DMF.[28] Interestingly, four sharp peaks at around 2900 cm^{-1} ($\nu_{s,\ as}$(C-H)) observed in the spectrum of the activated framework almost vanished upon occlusion of DMF, which is likely due to the interaction between guest molecules and the framework. As depicted in Fig. 1, the H atoms are located on the surface of the channel of *α*-$Mg_3(HCOO)_6$. Therefore, it is likely that the C-H bonds of the framework form weak C-H···O hydrogen bonding with the oxygen of DMF.

In the Raman spectrum of benzene loaded sample (Fig. 2 and Table 1), most of the fundamentals of benzene adsorbed in the MOF as well as several combinations and overtones were clearly observed. The bands at 609, 993 and 1176 cm^{-1} corresponding to the benzene ring deformation, ring breathing and C-H deformation modes.[29] The noticeable changes in the spectrum occurred in the C-H stretching region where the number of framework C-H stretching vibrations reduced from four sharp peaks to two broader peaks. Apparently, the different Raman profile in the C-H stretching region is mostly associated with the different polarity of guest molecules and thus the nature of the guest-framework interaction.

In the IR spectrum of benzene loaded framework, the new peak at 841 cm^{-1} of benzene loaded framework spectra is due to the free benzene δ_{op}(C-H) mode (Fig. 3). The similar frequency was also reported by Wang et al. for the spectra of benzene loaded in zeolite ZSM-5 by IR spectroscopy.[30] Their work shows that the adsorbed benzene molecule is only slightly perturbed from the D_{6h} point group symmetry of the free molecule. In the IR spectrum of DMF loaded framework, an absorption peak at a coincidentally similar frequency of 841 cm^{-1} can be interpreted as the free DMF δ_{op}(C-H).

Overall, as guest molecules, DMF and benzene can substantially affect the internal environment of the framework. For example, the two sharp peaks at 1610 and 1685 cm^{-1} of the framework become broader upon loading with guest molecules due to intermolecular interactions between the framework and the guests.

3.2. IR and Raman spectra of activated framework at high pressures

Raman spectra. Raman spectra of α-$Mg_3(HCOO)_6$ were collected from ambient pressure up to 3.83 GPa and then decompression to ambient pressure (Fig. 4a and 4b). The number of peaks in the Mg-O lattice mode region (100-350 cm^{-1}) gradually decreases with increasing pressure. When pressure is increased to 2.06 GPa and above, the number of the resolved peaks in the Mg-O lattice modes region is reduced from 11 to 2. However, the intensities of the Mg-O lattice modes are enhanced with increasing pressure. Similar phenomenon was also reported in an *in situ* high pressure Raman study of sodium formate (NaHCOO).[22] The dramatic changes in the number of Mg-O lattice modes and their intensities suggest a phase transition induced by pressure.

The significant changes in the ν_s(OCO) modes at 1375, 1398 and 1416 cm^{-1} were also observed. The three peaks remain very well resolved below 2.06 GPa (Fig. 4b). When pressure is increased above 2.06 GPa, the three ν_s(OCO) modes of the framework are gradually broadened and merge to a singlet peak. The strong C-H stretching modes become significantly broadened above 0.83 GPa. Further compression to 1.14 GPa leads to the splitting of the peak at 2898 cm^{-1} into two peaks at 2891 and 2903 cm^{-1}. All the C-H stretching modes become almost invisible above 2.06 GPa. The Raman data clearly indicate that α-$Mg_3(HCOO)_6$ undergoes a phase transition above 2.06 GPa. The Raman

spectrum of α-$Mg_3(HCOO)_6$ collected upon decompression shown in Figs. 4a and 4b looks distinctly different from the ambient spectra, which indicates that the structural change in α-$Mg_3(HCOO)_6$ framework induced by pressure is irreversible.

IR spectra. Although the Raman measurements revealed interesting irreversible structural transitions of activated framework when compressed to about 4 GPa, the extremely weak and broad Raman features beyond that pressure make it difficult to examine possible further transitions and framework stabilities at higher pressure region. In contrast, the strong IR absorption bands can be monitored at much higher pressures up to 12.55 GPa. The mid-IR spectra of α-$Mg_3(HCOO)_6$ upon compression to 12.55 GPa together with the spectrum of the recovered sample upon decompression to ambient pressure were collected in the region 600-3000 cm^{-1}, as shown in Fig. 5. Several changes in the IR spectra were obserevd. For instance, the ν_s(OCO) at 1379, 1385 and 1396 cm^{-1} first merged to a single peak at 1388 $cm^{-1}$when the sample was compressed to 0.86 GPa. A doublet at 1388 and 1409 cm^{-1} gradually merged to a singlet at 1432 cm^{-1} when the sample was compressed from 0.86 to 5.44 GPa. Furthermore, both peaks (1378 and 1432 cm^{-1}) seen at 5.44 GPa become weakened with increasing pressure to 12.55 GPa. These changes imply that the formate ligands bound to the metal may undergo distortion under high pressure. Interestingly, the recovered material exhibited a similar profile to the ambient spectrum. Since the mid-IR spectrum is more sensitive to the internal vibrations of organic linker and therefore provides information on organic linkers, the observed mid-IR spectra suggests that the formate ligands undergo distortion at higher pressure and this distortion is reversible. Thus, the IR data indicate that the MOF framework is distorted at a pressure as high as 12.55 GPa, but the topology remains intact.

The Raman spectrum of recovered material, on the other hand, is remarkably different from the ambient spectrum prior compression. This is particular true in the Mg-O lattice region, which is not accessible in mid-IR. Combination of mid-IR and Raman data, we suggest that pressure induces a phase transition in α-$Mg_3(HCOO)_6$. In the new phase, the overall topology of the MOF remains intact, but the framework and/or crystal symmetry undergo observable changes. The changes likely result mainly from the effect of pressure on the MgO_6 octahedra as the significant changes occur in the Mg-O lattice region of the Raman spectra. Upon decompression, the distortion involving organic linkers is reversed as seen in the mid-IR spectra, but the changes to the MgO_6 octahedra appear to be irreversible, judging from the Raman spectrum in Mg-O lattice region.

3.3. Raman and IR spectra of the MOF loaded with guest molecules at high-pressure

Raman spectra. Figs. 6 and 7 depict the selected Raman spectra of DMF and benzene loaded α-$Mg_3(HCOO)_6$ upon compression up to 4.0 GPa in the region of 50-3000 cm^{-1}. As the pressure is increased, all the peaks in both DMF and benzene loaded samples are broadened. Interestingly, unlike the situation for activated sample, the majority of the Mg-O lattice modes in 50-500 cm^{-1} for both DMF and benzene loaded framework do not show significant change in the entire pressure range, suggesting that no phase transition has occurred. This observation indicates that MOF framework containing guest species is much more stable to external pressure than that of the activated phase despite that the starting crystal structures of both activated and guest loaded frameworks are identical.[6] It appears that the observed stability results from the presence of guest species inside the pores. Such effects have been reported before.[31]

IR spectra. Fig. 8 shows the selected IR spectra of DMF and benzene loaded α-$Mg_3(HCOO)_6$ upon compression in the region of 600-3000 cm^{-1}. The spectra of both guest-loaded samples exhibit no dramatic change except that most of the peaks become broadened with increasing pressure. The recovered spectra of DMF and benzene loaded samples look almost identical to those recorded at ambient conditions. Therefore, the IR results are consistent with Raman data in that no phase transition occurs in DMF and benzene loaded frameworks.

3.4. Pressure effects on Raman and IR modes of activated and guest-loaded framework

To examine the possible phase transformations on compression, we monitored the Raman shifts and IR frequencies of activated framework and that loaded with DMF and benzene as a function of pressure, with details depicted in supporting information. The pressure coefficients (dν/dP (cm^{-1} GPa^{-1})) were calculated by linear regression of the experimental data, and the representative Raman and IR modes involving OCO vibrations are listed in Table 2. In general, most Raman modes exhibit pressure-induced blue shifts (Figs. S1, S2 and S3), indicating the bonds stiffen upon compression. For activated framework, no further slope changes other than the reduction of the number of lattice modes at 2 GPa were observed, indicating only one phase transition as discussed above. Additionally, the pressure coefficients (dν/dP) of DMF and benzene loaded frameworks are similar to those of the activated framework and no phase transitions can be identified for the guest loaded frameworks. Obviously, the bond strength is not very sensitive to

compression in a broad pressure region as the pressure coefficients are extremely small in magnitude (i.e., < 5 cm^{-1}/ GPa).

For IR measurements of activated and guest loaded frameworks, most of the IR modes also exhibited blue shifts with increasing pressure (Figs. S4, S5 and S6), consistent with Raman results. Compared to pressure-dependence of the Raman modes, it is interesting to note that for the framework carbonyl bending mode, a pressure coefficient as large as 11.7 (DMF-loaded smaple) and 17.6 cm^{-1} GPa^{-1} (benzene-loaded sample) was observed, which will be discussed below.

3.5. Discussion

The compression-decompression cycles on three α-$Mg_3(HCOO)_6$ systems reveal strongly contrasting transformation behavior and structural stabilities. Thus, in-depth understanding of possible high-pressure structures and guest-host interaction mechanisms are of fundamental interest. First of all, the Raman measurements suggest that activated α-$Mg_3(HCOO)_6$ framework exhibits high crystallinity upon compression to 4 GPa indicated by the well-resolved lattice modes. This is in a stark contrast to other MOFs investigated under high pressure, such as ZIF-8. Both Hu et al. and Moggach et al. reported that ZIF-8 undergoes a phase transition from a crystalline to a disordered or to an amorphous phase even upon slight compression to less than 2 GPa,[14, 18] suggesting that the α-$Mg_3(HCOO)_6$ framework has a substantially higher crystalline stability than ZIF-8. This observation is consistent with the fact that framework porosity of α-$Mg_3(HCOO)_6$ is significantly less than that of ZIF-8.

The reduction of the number of lattice modes of the empty framework upon

compression to 4 GPa indicates that the space group symmetry of the new crystalline phase is likely higher than monoclinic $P2_1/n$. Other known polymorphs of $Mg_3(HCOO)_6$ are the β and γ phases both with orthorhombic structures (space group $Pca2_1$ and $Pbcn$ respectively) [5]. In addition, both α– and β-$Mg_3(HCOO)_6$ have similar topology along the *b*-axis, where the 1D chains and 3D framework are formed by respective edge sharing and vertex sharing of the MgO_6 octahedra in both polymorphs[5]. More interestingly, the β angle for the $P2_1/n$ unit cell of α-$Mg_3(HCOO)_6$ is very close to 90° (i.e., 91.15°) at ambient pressure, suggesting a high possibility of structural modification by compression to a higher crystal symmetry such as orthorhombic. The recovery of the new high-pressure polymorph indicates that this polymorph might be thermodynamically favored over the α-phase at high pressures. Nonetheless, the detailed structure of this new polymorph or possibility of the pressure-induced transformation to γ-$Mg_3(HCOO)_6$ form needs to be verified by X-ray diffraction.

Secondly, the frameworks responded to external compression differently between empty and guest-loaded situations. Similar to the empty framework, guest-loaded α-$Mg_3(HCOO)_6$ also undergoes pressure-induced structural modifications but remains crystalline instead of becoming amorphous as ZIF-8. However, the similar lattice profiles between 4 GPa and ambient pressure suggest that there is no major change in the space group of the framework, other than slight distortion. Furthermore, the complete structural reversibility of the pressure-induced modifications of the guest-loaded frameworks as indicated by the almost identical Raman and IR profiles before and after compression suggests guest molecules played an important role in enhancing the structural stability of framework. This observation is consistent with the previous studies on Cu-btc in the

presence of different pressure transmitting media where the compressibility and transition pressures were found strongly dependent on the type of media.[11] Similarly, ZIF-8 framework was also found to become more stable when loaded with penetrating transmitting medium or CO_2.[8, 18] Thus, it is likely a general trend that guest molecules can significantly enhance framework resistance to external stress, independent of the guest molecules loaded. Such behavior was also observed in other porous materials such as zeolites.[29, 32]

Of particular interest is the correlation between the rigidity of the framework and the microscopic responses of the framework to external stress. For instance, a previous study of (4-chloropyridinium)$_2$[CoX_4] (X=Cl, Br) at high pressures using X-ray diffraction has allowed the understanding of the correlation between the preferential compressible direction of the framework and the contribution of the $\pi - \pi$ stacking and the halogen−halogen (dispersion) interactions.[17] In this study, based on the known starting structure of α-$Mg_3(HCOO)_6$, among the four types of MgO_6 octahedral clusters, MgO_6 involving Mg2 and Mg4 are likely more susceptible to displacement upon external stress compared to MgO_6 involving Mg1 and Mg3, contributing to the distortion of the framework (Fig. 1). This is not only because of their coordination environments, but also their locations in the 1D chains of the frame as well as the overall topology. Since the chelation by μ^2-O is typically stronger than μ^1-O, the structural rigidity of the individual clusters is different based on the ratio of μ^2-O over μ^1-O, resulting in Mg1-oxygen cluster being most rigid (with Mg^{2+} bound to six μ^2-O), and Mg2- and Mg4-oxigen clusters least rigid (with Mg^{2+} bound to four μ^1-O). Therefore, the distortion of the framework may be initiated by the distortion of the individual Mg2 and Mg4 clusters. In addition, Mg2 and

Mg4 are located on the edge center of the 1D chains on the *ac* plane. As a result, these units are more prone to displacement upon external compression than those located at the vertices (i.e., Mg1 and Mg3) due to the different topological constraint. Although in diamond anvils, materials are typically compressed isotropically, uniaxial compression is expected for anisotropic framework structures such as α-$Mg_3(HCOO)_6$ with one-dimensional channel along *b*-axis. Thus the compression is most likely rendered along vectors on the ac plane. If the above-mentioned pressure-driven symmetry enhancement is taken into consideration, larger displacement magnitude for Mg4 than Mg2 will facilitate the formation of an orthorhombic lattice. Correspondingly, Mg4-oxygen clusters will likely displace perpendicularly to the chain edge while Mg2 along the chain edge, as indicated by the arrows in Fig. 1, to accommodate such a uniaxial compression. Such motions will necessarily results in more prominent distortions of the Mg4 clusters. As a result, the Mg-O and associated carbonyl groups might be significantly influenced. Indeed, the remarkably large pressure dependence of one of the symmetric bending mode of carbonyl group for DMF and benzene loaded α-$Mg_3(HCOO)_6$ framework might be attributed to this proposed mechanism. Again, the detailed pressure induced structural evolutions need to be verified by in situ X-ray diffraction.

Finally, understanding the guest-selective host-guest interaction under external stress is of great importance for further storage applications of the *α*-$Mg_3(HCOO)_6$. Ample examples have shown that different guest molecules can substantially alter the framework structure in other porous materials such as zeolite (e.g., ZSM-5).[28] In the current work, we deliberately chose two very different guest molecules in terms of molecular size and polarity to examine their influence on the framework under

compression conditions. Apparently, the size difference between benzene and DMF only resulted in different initial expansion of unit cell by 4%,[6] while no significantly different pressure behavior is observed upon compression. In addition, there is no particular correlation between structural stability and either polar or non-polar guest molecules. These observations suggest that guest-host interaction is primarily determined by the initial loading state (in both cases, the guest molecule occupies the cavity with a 1:1 ratio and in already predetermined crystallographic orderness), while the nature of the interaction is not pressure dependent in the examined pressure region. The adsorption tests of H_2, N_2 on α-$Mg_3(HCOO)_6$ [6] and of CO_2 on both α- and γ-$Mg_3(HCOO)_6$ [5] showing similar intake performance suggest that the guest-host interaction is not guest selective and mainly regulated by framework porosity. Thus the intrinsic rigidity of the framework making the large cavity occluding guest molecules resilient to compression makes the investigation of additional intake of CO_2 at much higher pressures than ambient an interesting possibility. Indeed, ZIF-8 is found to have a substantially improved performance of CO_2 intake in the pressure range similar to the current study. Furthermore, α-$Mg_3(HCOO)_6$ framework composed of exclusively carbonyl linkers can be considered as substantial CO_2 moiety already in the framework. The chemical and mechanical stability suggests strong affinity between CO_2 and Mg^{2+}, making additional intake of CO_2 into the framework highly thermodynamically favorable. As a matter of fact, other Mg based MOF with open metal sites such as CPO-27-Mg and Mg-MOF-74 both exhibited a remarkably high uptake of ~70%wt CO_2 even at ambient conditions. [7, 32-35]

4. Conclusions

In situ IR and Raman spectroscopic measurements of α-$Mg_3(HCOO)_6$ framework, as well as DMF and benzene loaded framework were investigated under high external pressures up to 13 GPa. The activated α-$Mg_3(HCOO)_6$ framework structure was found chemically stable under compression up to 13 GPa, while an irreversible crystal-to-crystal structural transition was observed above 2 GPa. In contrast, IR and Raman spectra show that unlike the acitvated framework, α-$Mg_3(HCOO)_6$ fameworks loaded with DMF and benzene exhibit no obvious structual transition and the pressure behavior of the guest loaded framework is completely reversible. These observations suggest that pressure stability of the α-$Mg_3(HCOO)_6$ famework can be enhanced upon guest loading. The possible new high-pressure structure of the activated framework and corresponding transition mechanism were analysized based on framework topology and Mg-O coordination configurations. The contrasting high pressure stabilities between empty and loaded framework, together with the high affininty between framework and CO_2 makes the α-$Mg_3(HCOO)_6$ a promsing MOF for green gas stroage under pressure loading conditions.

Acknowledgments

This work was partially funded by the Doctorate Fellowship Foundation (163020070) and the Scientific Research Foundation for Advanced Talents of Nanjing Forestry University (GXL2014035); the Natural Science Foundation of China (31100417 and 31300482), and Jiangsu province Science Foundation for Youths (BK20130975 and BK20130966), China; Priority Academic Program Development of Jiangsu Higher Education Institutions,. Y.H. and Y.S. acknowledge the Natural Science and Engineering Research Council of Canada (NSERC) for Discovery Grants. Funds from the Canada Research Chair program (Y.H.), an NSERC Discovery Accelerator Award (Y.H.), a Leading Opportunity Fund from the Canadian Foundation for Innovation (Y.S.), and an Early Researcher Award from the Ontario Ministry of Research and Innovation (Y.S.) are also gratefully acknowledged.

References

1. S. Kitagawa, R. Kitaura and S. Noro, *Angew. Chem. Int. Edit.*, 2004, **43**, 2334-2375.
2. M. Gimeno-Fabra, A. S. Munn, L. A. Stevens, T. C. Drage, D. M. Grant, R. J. Kashtiban, J. Sloan, E. Lester and R. I. Walton, *Chem. Commun.*, 2012, **112**, 673-1268.
3. R. J. Kuppler, D. J. Timmons, Q. R. Fang, J. R. Li, T. A. Makal, M. D. Young, D. Q. Yuan, D. Zhao, W. J. Zhuang and H. C. Zhou, *Coordin. Chem. Rev.*, 2009, **253**, 3042-3066.
4. J. Xu, V. V. Terskikh and Y. N. Huang, *Chem. Eur. J.*, 2013, **19**, 4432-4436.
5. A. Mallick, S. Saha, P. Pachfule, S. Roy and R. Banerjee, *Inorg. Chem.*, 2011, **50**, 1392-1401.

6. J. A. Rood, B. C. Noll and K. W. Henderson, *Inorg. Chem.*, 2006, **45**, 5521-5528.
7. D. Britt, H. Furukawa, B. Wang, T. G. Glover, O. M. Yaghi and J. Halpern, *P. Natl. Acad. Sci. U.S.A.*, 2009, **106**, 20637-20640.
8. Y. Hu, Z. Liu, J. Xu, Y. Huang and Y. Song, *J. Am. Chem. Soc.*, 2013, **135**, 9287-9290.
9. A. J. Graham, D. R. Allan, A. Muszkiewicz, C. A. Morrison and S. A. Moggach, *Angew. Chem. Int. Edit.*, 2011, **50**, 11138-11141.
10. A. J. Graham, J. C. Tan, D. R. Allan and S. A. Moggach, *Chem. Commun.*, 2012, **48**, 1535-1537.
11. K. W. Chapman, G. J. Halder and P. J. Chupas, *J. Am. Chem. Soc.*, 2008, **130**, 10524-10526.
12. K. W. Chapman, D. F. Sava, G. J. Halder, P. J. Chupas and T. M. Nenoff, *J. Am. Chem. Soc.*, 2011, **133**, 18583-18585.
13. K. W. Chapman, G. J. Halder and P. J. Chupas, *J. Am. Chem. Soc.* , 2009, **131**, 17546-17547.
14. Y. Hu, H. Kazemian, S. Rohani, Y. Huang and Y. Song, *Chem. Commun.*, 2011, **47**, 12694-12696.
15. T. D. Bennett, J. C. Tan, S. A. Moggach, R. Galvelis, C. Mellot-Draznieks, B. A. Reisner, A. Thirumurugan, D. R. Allan and A. K. Cheetham, *Chem. Eur. J.*, 2010, **16**, 10684-10690.
16. D. Fairen-Jimenez, S. A. Moggach, M. T. Wharmby, P. A. Wright, S. Parsons and T. Duren, *J. Am. Chem. Soc.*, 2011, **133**, 8900-8902.

17. G.M. Espallargas, L. Brammer, D.R. Allan, C.R. Pulham, N. Robertson and J.E. Warren, *J. Am. Chem. Soc.,*2008, **130**, 9058–9071.

18. S. A. Moggach, T. D. Bennett and A. K. Cheetham, *Angew. Chem. Int. Edit.*, 2009, **48**, 7087-7089.

19. H. K. Mao, J. Xu and P. M. Bell, *J Geophys. Res.-Solid*, 1986, **91**, 4673-4676.

20. Z. H. Dong and Y. Song, *J. Phys. Chem. C.*, 2010, **114**, 1782-1788.

21. V. Koleva and D. Stoilova, *J. Mol. Struct.*, 2002, **611**, 1-8.

22. A. M. Heyns, *J. Chem.P*, 1986, **84**, 3610-3616.

23. M. C. Bernard, V. Costa and S. Joiret, *E Preserv. Sci.*, 2009, **6**, 101-106.

24. M. Pohl, A. Pieck, C. Hanewinkel and A. Otto, *J. Raman Spectrosc.*, 1996, **27**, 805-809.

25. D. Stoilova and V. Koleva, *J. Mol. Struct.*, 2000, **553**, 131-139.

26. T. Cottineau, M. Richard-Plouet, J. Y. Mevellec and L. Brohan, *J. Phys. Chem. C.*, 2011, **115**, 12269-12274.

27. S. K. Park, K. C. Min, C. Lee, S. K. Hong, Y. Kim and N. S. Lee, *B. Korean Chem. Soc.*, 2009, **30**, 2595-2602.

28. X. F. Zhou, J. A. Krauser, D. R. Tate, A. S. VanBuren, J. A. Clark, P. R. Moody and R. F. Liu, *J. Phys. Chem.*, 1996, **100**, 16822-16827.

29. Y. N. Huang and E. A. Havenga, *J. Phys. Chem. B.*, 2000, **104**, 5084-5089.

30. H. P. Wang, T. Yu, B. A. Garland and E. M. Eyring, *Appl. Spectrosc.*, 1990, **44**, 1070-1073.

31. J. S. Tse, D. D. Klug, *Science*, 1992, **255** 1559-1561.

32. Y. Q. Fu, Y. Song and Y. I. Huang, *J. Phys. Chem. C.*, 2012, **116**, 2080-2089.

33. D. Britt, H. Furukawa, B. Wang, T. G. Glover and O. M. Yaghi, *P. Natl. Acad. Sci. U.S.A.*, 2009, **106**, 20637-20640.

34. X. Q. Kong, E. Scott, W. Ding, J. A. Mason, J. R. Long and J. A. Reimer, *J. Am. Chem. Soc.*, 2012, **134**, 14341-14344.

35. J. B. DeCoste, G. W. Peterson, B. J. Schindler, K. L. Killops, M. A. Browe and J. J. Mahle, *J. Mater. Chem. A*, 2013, **1**, 11922-11932.

Table 1. Assignments of selected vibrational bands of the Raman and IR modes of activated and guest-loaded α-$Mg_3(HCOO)_6$.

Raman (cm^{-1})			IR (cm^{-1})					Assignment [a]
Activated sample	DMF loaded sample	Benzene loaded sample	Activated sample	DMF loaded sample	Benzene loaded sample	α-$Mg_3(HCOO)_6$ loaded with DMF [b]	$Mg(HCOO)_2 \cdot 2H_2O$ [c]	
			619	604	604	662		δ_s (OCO)
			700	701	703	722		δ_s (OCO)
779, 792	785	755, 792	767	765	766	790	745, 761	δ_s (OCO)
				841	841			δ_{op} (C-H)
1064	1094	1079				1099, 1259		ρ_{op} (C-H)
1357	1357	1365	1366	1366	1366			ν_s (OCO)
1375	1376	1374	1379	1375	1375	1376	1375	ν_s (OCO)
	1386	1385	1385	1383	1383		1382	ν_s (OCO)
1398	1395	1394	1396	1395	1395	1396	1392, 1395	ν_s (OCO)
1416	1405	1404	1406	1405	1405	1417, 1460	1406	ν_s (OCO)
1630	1632		1610	1605	1601	1608	1600, 1615	ν_{as} (OCO)
1686, 1690	1664,1687		1685	1684	1685	1670		ν_{as} (OCO)
2879, 2898	2890	2888	2894	2891	2892	2854	2891	$\nu_{s, as}$ (C-H)
2931	2904	2902	2910	2906	2907	2924	2907	$\nu_{s, as}$ (C-H)

[a] ν–stretching (symmetric and anti-symmetric); δ-bending (symmetric and anti-symmetric or in plane and out of plane); ρ–rocking (in plane and out of plane). Reference 21, 25-27

[b] Reference 6

[c] Reference 24

Table 2. Pressure dependences [dv/d*P*(cm^{-1} GPa^{-1})] of the selected IR and Raman bands involving carbonyl (OCO) group of activated and guests loaded α-$Mg_3(HCOO)_6$ on compression.

Assignment	Raman				IR			
	Wavenumber [a] (m^{-1})	Activated	Loaded with DMF	Loaded with benzene	Frequency [a] (m^{-1})	Activated	Loaded with DMF	Loaded with benzene
δ_s (OCO)	779	3.1	1.9	3.9	700	7.5	0.5	0.2
δ_s (OCO)					767	7.5	0.6	0.1
δ_s (OCO)	792	3.6	4.5	4.2	844	6.5	11.1	17.6
ν_s (OCO)	1357	2.8	3.2	4.5	1366	5.1	5.8	6.0
ν_s (OCO)	1375	2.4	4.0	4.8	1379	13.1	1.5	1.7
ν_s (OCO)					1385	4.1	3.5	2.0
ν_s (OCO)	1398	0.7	1.8	4.8	1396	2.6	2.9	2.7
ν_s (OCO)	1416	0.6	1.2	1.9	1406	3.2		2.4
ν_{as} (OCO)	1630	1.5	2.8		1610	3.0	0.9	3.3
ν_{as} (OCO)	1686	1.2	3.2		1685	4.0	2.7	0.2

[a] refers to the activated sample.

Figure Captions

Fig. 1 Extended framework structure of α-$Mg_3(HCOO)_6$ MOF viewed along *b* axis (a) and local geometries showing different oxygen coordinations on carbon (b) and octahedrally coordinated Mg clusters with different coordination environments for Mg (c). The four types of Mg are labeled on the frame and in the cluster. The colored balls denote atoms of magnesium (black), oxygen (red), carbon (cyan) and hydrogen (blue). The dashed arrows indicate possible displacement direction for Mg4 (larger magnitude) and Mg2 (smaller magnitude) upon external compression (see text).

Fig. 2 Selected Raman spectra of activated, DMF and benzene loaded framework in the region of 0-3000 cm^{-1} at ambient pressure, the lattice region with enhanced intensity 50-1200 cm^{-1} (a) and 1370-3000 cm^{-1} (b). The omitted spectral regions are due to the diamond peak and lack of spectroscopic features.

Fig. 3 Selected IR spectra of activated, DMF and benzene loaded framework in the region of 600-3000 cm^{-1} at ambient pressure.

Fig. 4 Selected Raman spectra of activated α-$Mg_3(HCOO)_6$ on compression to a highest pressure of 3.83 GPa in the region of 50-3000 cm^{-1}, the lattice region with enhanced intensity 50-1200 cm^{-1} (a) and 1370-3000 cm^{-1} (b) at pressures of 0-3.83 GPa. The relative intensities are normalized and thus are directly comparable.

Fig. 5 Selected IR spectra of activated α-$Mg_3(HCOO)_6$ on compression to a highest pressure of 12.55 GPa and as recovered. The relative intensities are normalized and thus are directly comparable.

Fig. 6 Selected Raman spectra of DMF α-$Mg_3(HCOO)_6$ on compression to a highest pressure of 4.0 GPa in the region of 0-3000 cm^{-1}, the lattice region with enhanced intensity 50-1200 cm^{-1} (a) and 1370-3000 cm^{-1}(b) at pressures of 0-4.0 GPa. The relative intensities are normalized and thus are directly comparable.

Fig. 7 Selected Raman spectra of benzene loaded α-$Mg_3(HCOO)_6$ on compression to a highest pressure of 4.0 GPa in the region of 0-1200 cm^{-1}, the lattice region with enhanced intensity (a) 1370-3000 cm^{-1} and (b) at pressures of 0-4.74 GPa. The relative intensities are normalized and thus are directly comparable.

Fig. 8 Selected IR spectra of DMF loaded (a) and benzene loaded (b) α-$Mg_3(HCOO)_6$ on compression to a highest pressure of 12.40 GPa and as recovered. The relative intensities are normalized and thus are directly comparable.

Fig 1

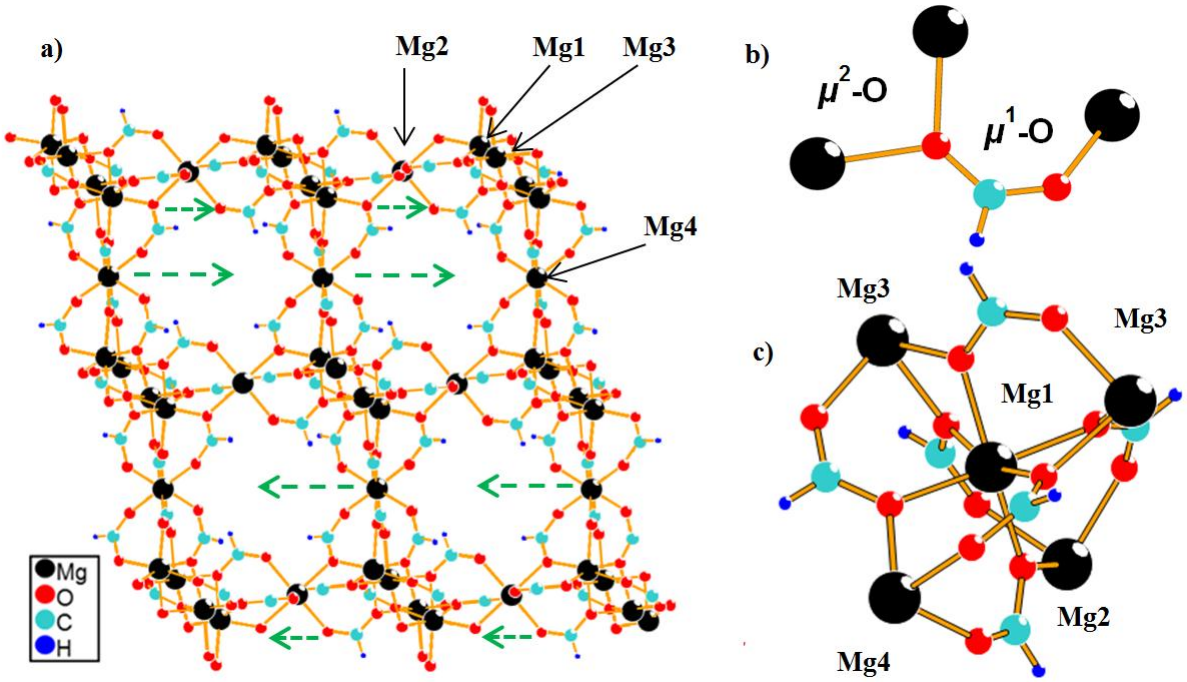

Fig 2

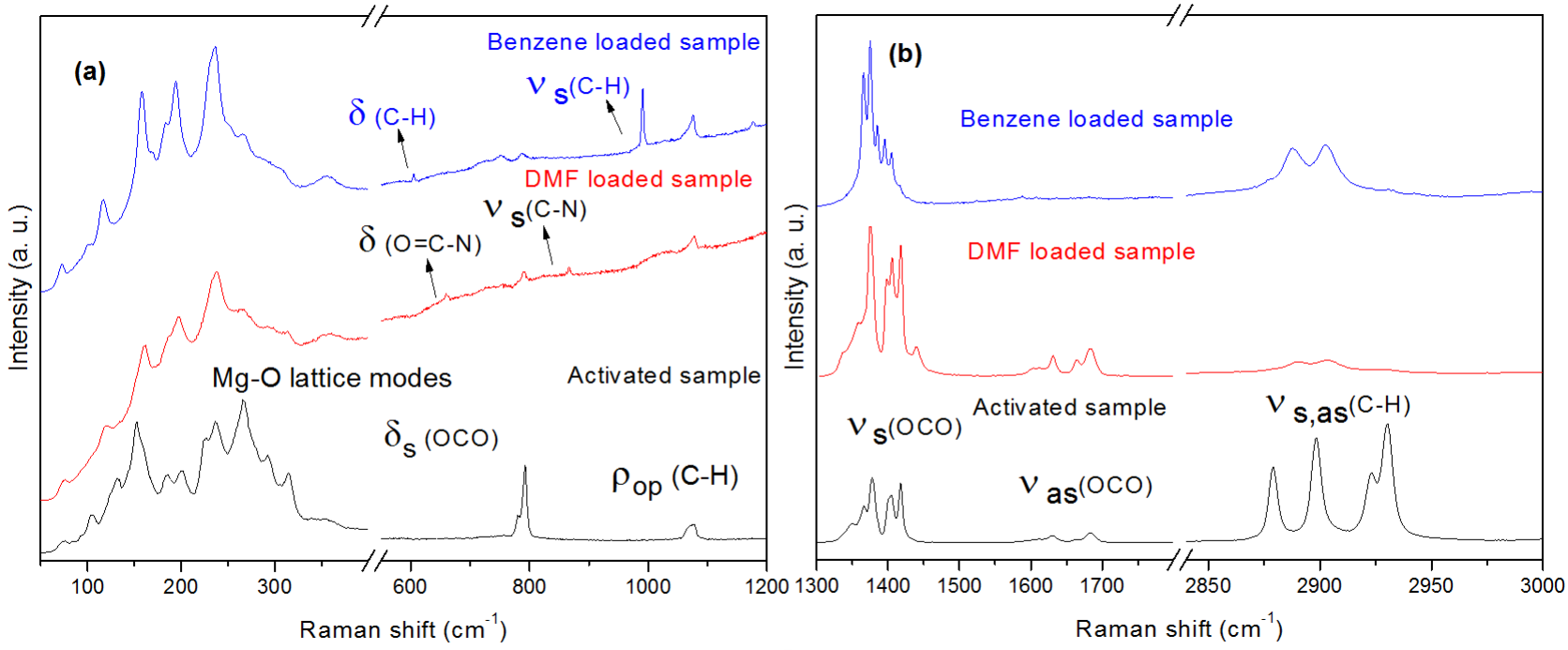

Fig 3

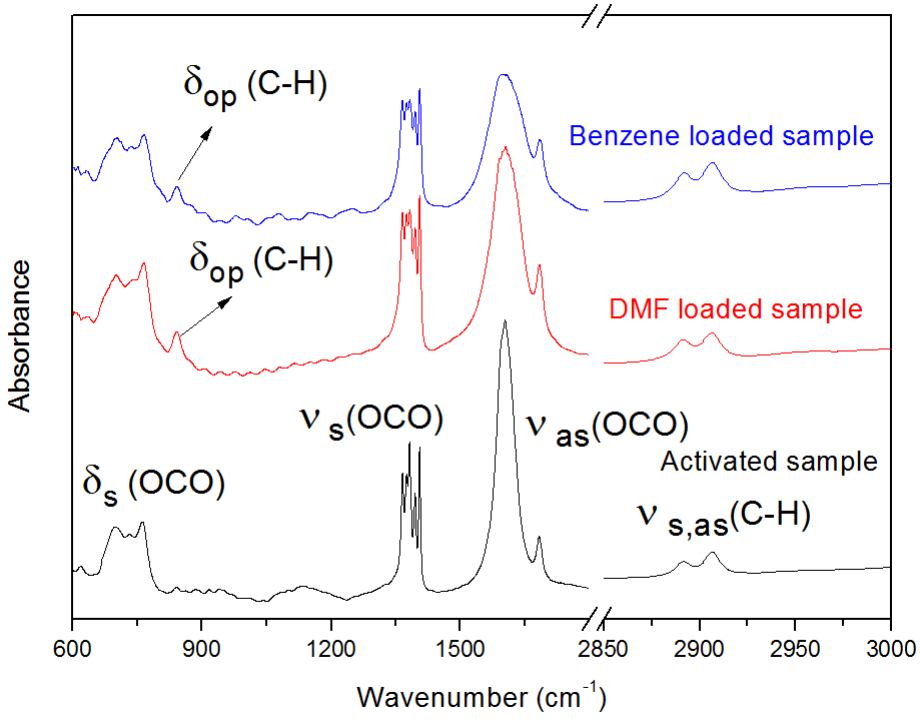

Fig 4

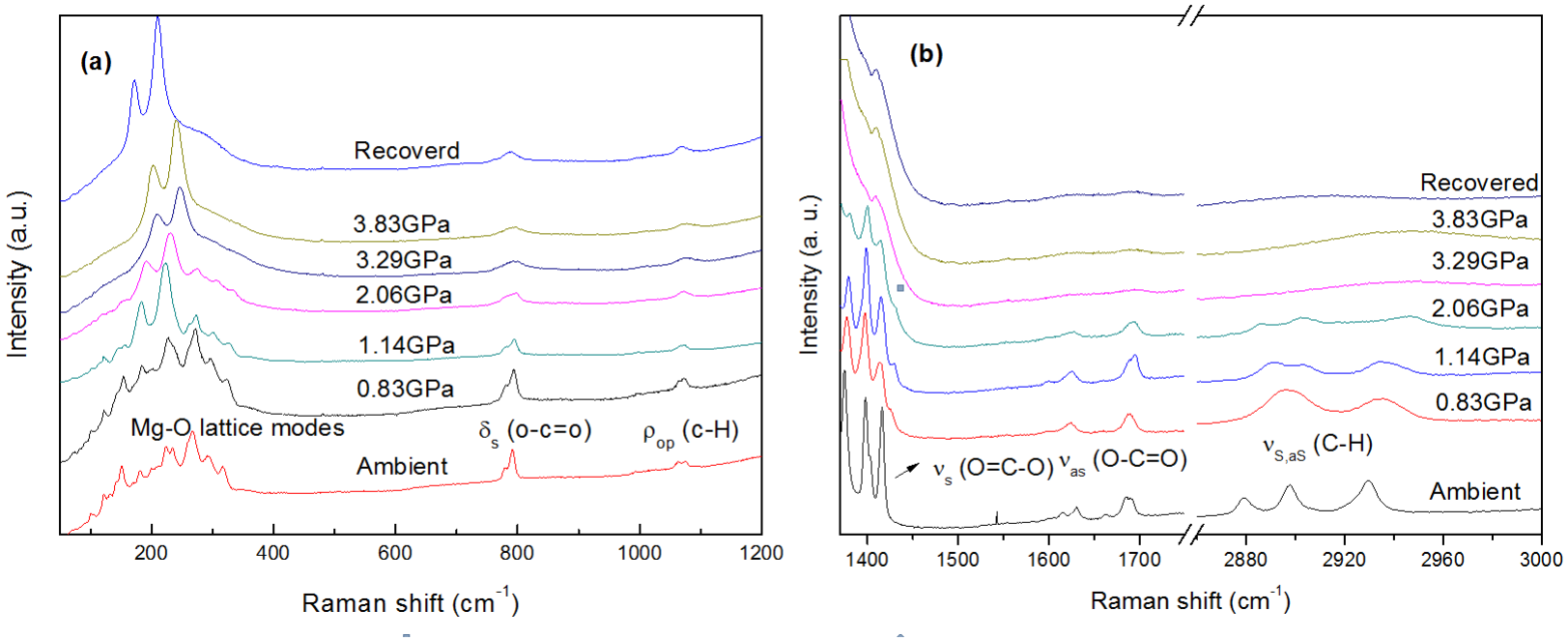

Fig 5

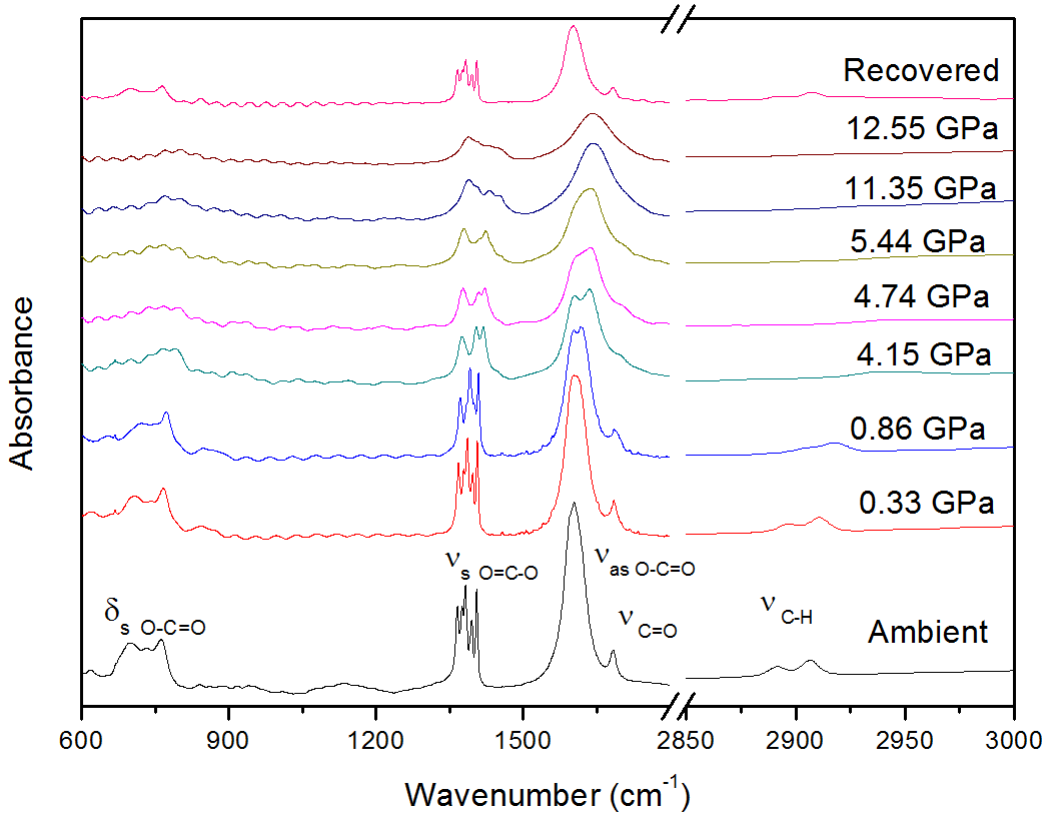

Fig 6

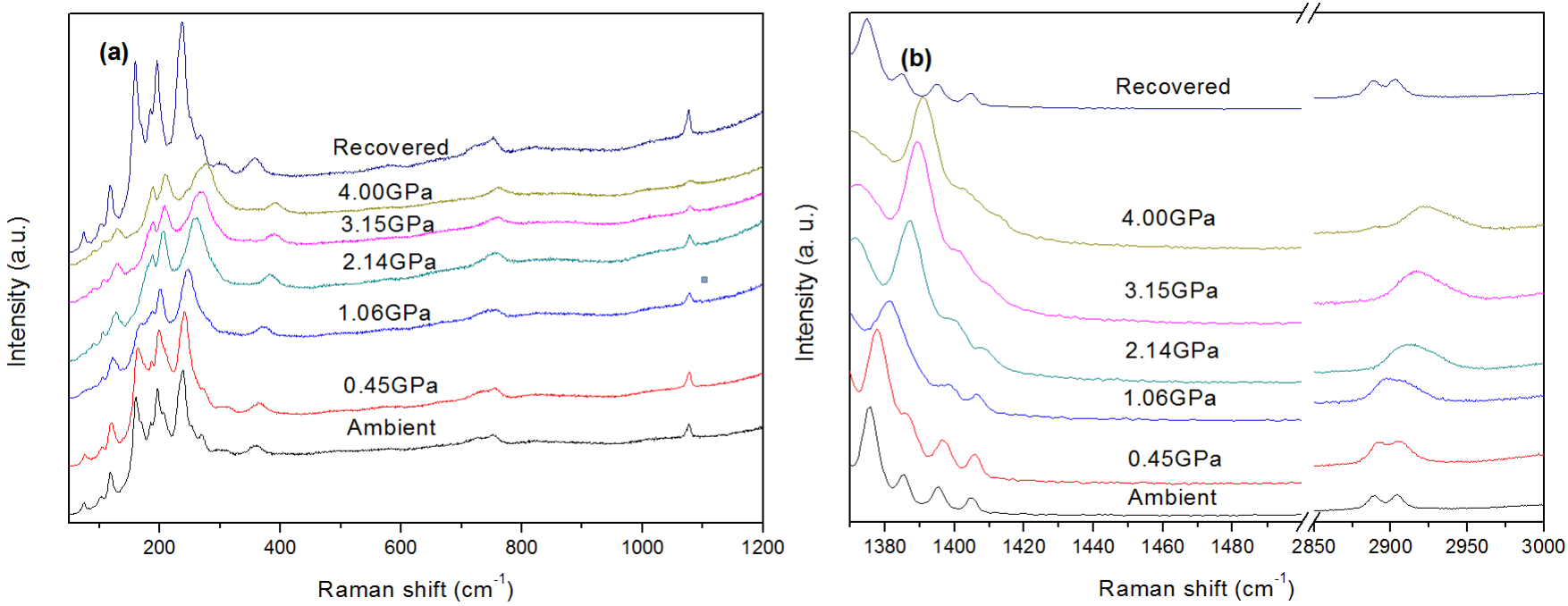

Fig 7

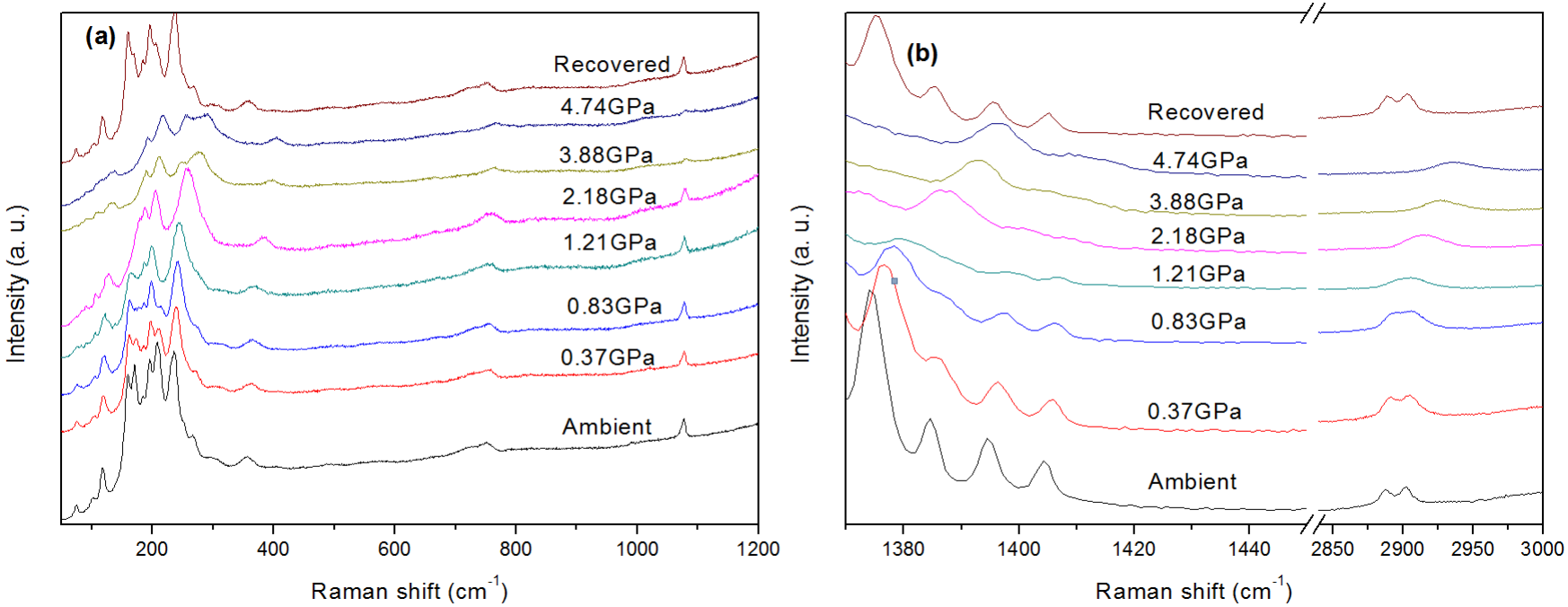

Fig 8

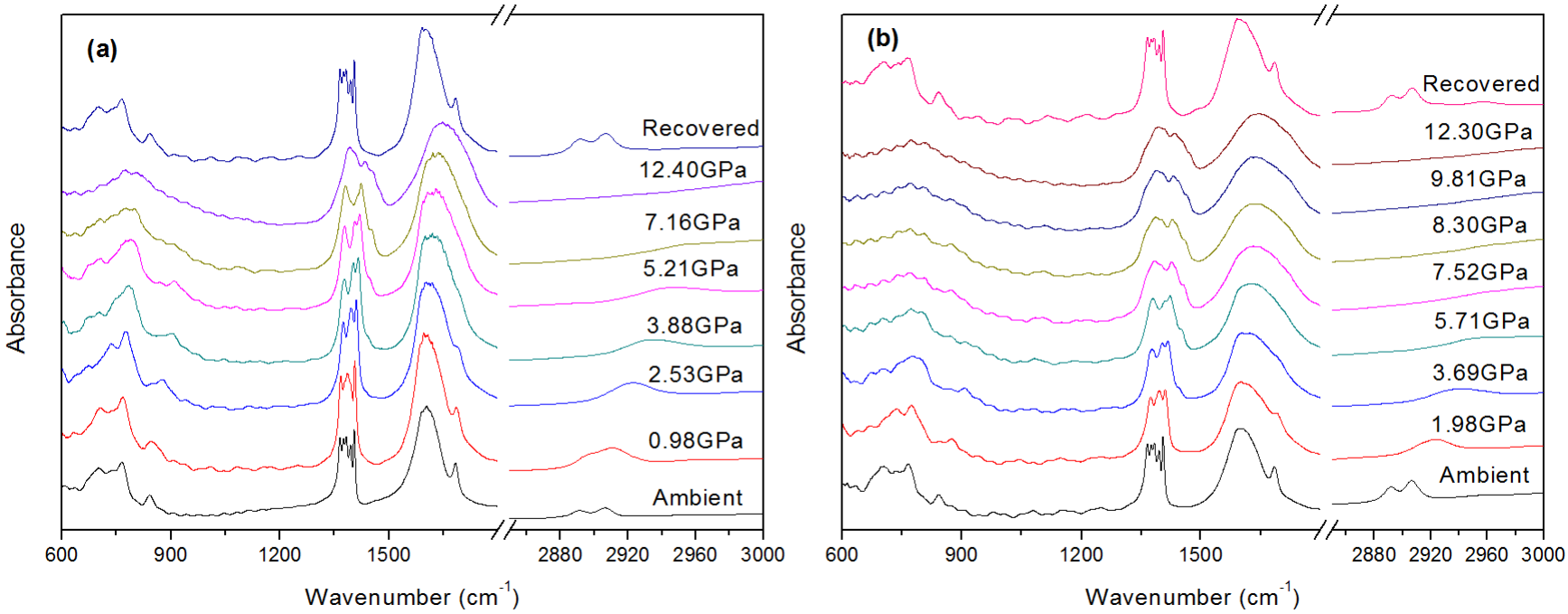

TOC Graphic

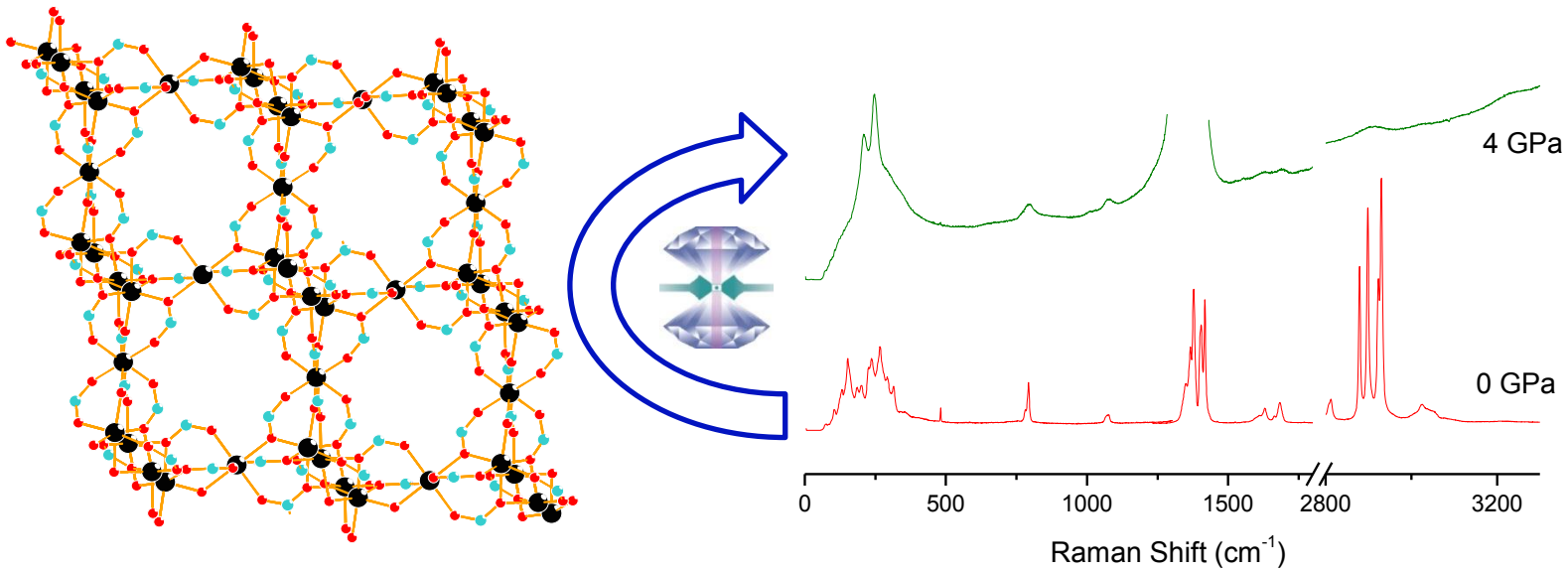

First high-pressure study on MOF α-$Mg_3(HCOO)_6$ probed by *in situ* vibrational spectroscopy revealed strongly contrasting host-dependent structural transitions and stabilities.